

## Investigations on Disturbance Amplification in a Laminar Separation Bubble by Means of LDA and PIV

By

M. Lang, U. Rist, S. Wagner

Institut für Aerodynamik und Gasdynamik der Universität Stuttgart

Pfaffenwaldring 21, 70550 Stuttgart, Germany

E-Mail: [lang@iag.uni-stuttgart.de](mailto:lang@iag.uni-stuttgart.de)

<http://www.iag.uni-stuttgart.de>

### ABSTRACT

Laminar-turbulent transition is an important feature in aerospace aerodynamics because of its influence on fuel consumption via the drag. Despite many years of research on fundamental mechanisms of the transition process in many generic configurations relevant for aircrafts, as well as other applications, there are situations which are less well understood and hence much more difficult to predict than certain "standard" cases, as e.g. zero-pressure gradient flat-plate boundary-layer transition. When a laminar boundary layer separates due to an adverse streamwise pressure gradient, the flow is subject to increased instability with respect to small-amplitude disturbances. Laminar-turbulent transition will occur, and in the considered case of a laminar separation bubble (LSB), the turbulent boundary layer will reattach.

The experiments were carried out in a laminar water-tunnel. The low turbulence level allows investigations on the development of intentionally excited 2-D or 3-D disturbance-wave combinations under controlled conditions. With respect to the disturbance source, the development of such perturbations within the separated boundary layer is measured by means of phase-averaged Laser-Doppler-Anemometry (LDA) and phase-locked Particle Image Velocimetry (mono-PIV and stereoscopic-PIV (SPIV)).

The role of unsteady disturbances with (3-D) and without (2-D) controlled spanwise variation in the occurring mechanism of transition is examined in detail. The transition mechanism occurring in the flow-field under consideration will be discussed and observations for the development of small disturbances are compared to direct numerical simulations (DNS) and predictions from linear stability theory (LST).

A method will be shown to measure wall-normal amplitude distributions and amplification rates of essentially small, unsteady (periodical) 3D disturbance waves within the boundary layer by means of phase-locked mono-PIV. By sequentially shifting the phase angle with respect to the disturbance source over one fundamental period, instantaneous boundary-layer profiles were measured. In order to also capture spanwise wave lengths in case of 3-D disturbance input, the flow field was scanned automatically with the light sheet in this direction for each phase angle. A double Fourier transform in time (fundamental period) and spanwise direction then yields the amplitudes and phases of the disturbance modes. Results are compared in detail with corresponding LDA measurements and linear stability theory. With the possibility of measuring unsteady disturbance development by PIV the measurement time could be significantly decreased by at least a factor of ten in comparison to adequate phase-averaged LDA measurements.

## 1. INTRODUCTION

The occurrence of boundary-layer separation can essentially affect the efficiency of a whole system via the drag, e.g. the wing of a sailplane or commercial aircraft. In the latter case the Reynolds number for a deployed slat lies in the same range as for a wing of a sailplane. Beside its influence on drag, the occurrence of a LSB causes noise. This is an important aspect e.g. in consideration of wind-turbine blades.

Despite several fundamental experimental (e.g. Gaster, 1966, Fitzgerald and Müller, 1988 and Watmuff, 1999) and numerical (e.g. Maucher et al., 1999 and Spalart and Strelets, 2000) investigations on transition in a laminar separation bubble it is still difficult to predict and understand processes leading to breakdown of the separated shear layer. The experiments were carried out in a laminar water-tunnel which was especially designed to study transition in Blasius boundary layers and in separation bubbles (Strunz and Speth, 1987). Wiegand (1997) investigated boundary layer transition initiated by a point source using hot-film anemometry. Thereby, he also confirmed the high quality of the tunnel flow with a turbulence level of less than 0.05%. The low turbulence level in the free stream allows investigations on amplification of intentionally excited disturbances and their influence on transition. Because of large temporal and spatial scales in water, this facility is particularly suitable for high resolved measurements and also for flow visualization. The good optical access to the test section allows PIV measurements in all cartesian planes of the flow field. Due to the sensitivity of the transition process, both applied non-intrusive measurement techniques (LDA and PIV) are suitable and reliable instruments for quantitative flow characterisation.

## 2. EXPERIMENTAL SET-UP

A flat plate with an elliptical leading edge is mounted in the test section of the laminar water tunnel. At the end of the flat plate a screen leads to a pressure difference between the upper and the lower side. Therefore, fluid transport is forced through a gap between the flat plate and the tunnel side-walls. This prevents the formation of an unstable corner boundary-layer, therefore extending the range of laminar flow on the plate. At a free stream velocity of  $u_8 = 125 \text{ mm/s}$ , an average shape factor of  $H_{12} = 2.6$  was measured in spanwise direction (zero pressure gradient). Within a range of  $-200 \text{ mm} < z < 200 \text{ mm}$  it varies only about  $\pm 1\%$ . Therefore, the boundary layer can be assumed to approximately a two dimensional boundary-layer.

To generate a pressure induced laminar separation bubble, a displacement body is positioned in the test section above the plate (figure 1). After a short region of favourable pressure gradient, the adverse pressure gradient is applied. This is a common technique and was also used by Gaster (1966). In the laminar water tunnel, a displacement body with a simple triangular shape is used. The cross section ratio of 1:1.43 and an opening angle of  $5.1^\circ$  after the narrowest section under the displacement body were first chosen according to streamwise applied pressure distributions from available DNS data (Maucher et al., 1999). Finally, these parameters were adjusted by flow visualization. To allow high resolution measurements the separation bubble had to have a certain size, but it had not to become too large because of long measurement times in water with the LDA. The boundary layer developing on the displacement body is sucked off in the narrowest section and through another suction strip in the region of adverse pressure gradient. This prevents separation and transition on the displacement body itself. The necessary suction rate was established by flow visualization.

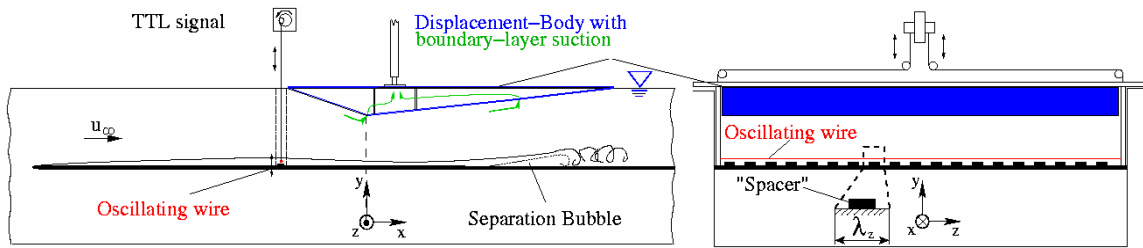


Fig. 1 Experimental set-up in the test section of the laminar water-tunnel.

The experiment is performed under controlled conditions. To investigate the development of an intentionally applied disturbance a 2-D Tollmien-Schlichting wave (TS-wave) is enforced by an oscillating wire. Its power unit generates a TTL trigger-signal each period, which is taken as time reference for phase-locked and phase-averaged measurements. The wire is positioned in the critical layer in region of favourable pressure gradient. The frequency of the disturbance input is  $f_0=1.1 \text{ Hz}$ . It was chosen to match the most amplified frequency according to linear stability theory. In the undisturbed case vortex shedding occurs with the same frequency but with amplitudes varying in time when compared to the case with disturbance input.

In order to introduce a 3-D disturbance, thin ( $1.0 \text{ mm}$ ) metal plates are placed regularly underneath the wire. These so called "spacers" cause a steady 3-D disturbance mode which interacts with the TS-wave. This results in a three-dimensional wave combination with typical peak-valley structure (figure 2a), where the boundary layer thickens stronger in the peak plane compared to the valley plane (Klebanoff et al., 1962, Kruse and Wagner, 1996 and Kruse, 1997). An advantage of 3-D disturbance input is that vortex structures, appearing with the onset of transition, are fixed in spanwise direction. In the present measurements with 3-D disturbance input, the spanwise wavelength was set to  $\lambda_z=58 \text{ mm}$ , so that regularly appearing spanwise vortex structures could be seen in the transition region (figure 2b). Flow visualizations using the hydrogen bubble technique were carried out to determine the spanwise wavelength. For figure 2b a mirror was positioned beneath the flat plate. Thus, a simultaneous view of the  $xy$ - and  $xz$ -plane is shown.

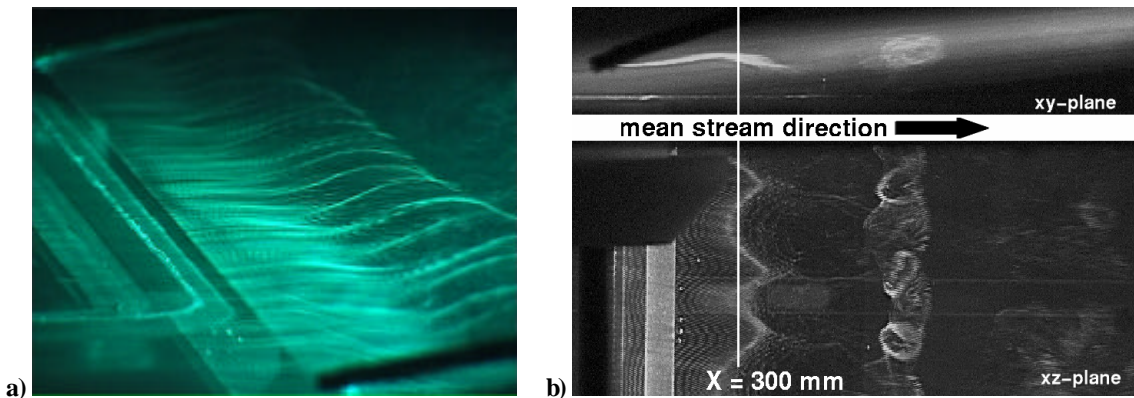


Fig. 2 Flow visualization in the transition region of the separated shear layer with hydrogen bubbles.

- a) 3-D disturbance wave.
- b) Shear layer roll-up with 3-D vortex shedding.

The applied 2-component LDA is a Dantec system and measures the velocity components  $u(t)$  in mean flow direction and  $v(t)$  perpendicular to the flat plate (Kruse and Wagner, 1996). In contrast to hot-film anemometry, the possibility to identify velocities with their value and direction by LDA is an important benefit in the transition region of the separated shear layer with its strong bidirectional velocity fluctuations. Thus, the dividing streamline can be determined directly from the measured velocity profiles.

The PIV system was built up in corporation with the “Deutsches Zentrum für Luft- und Raumfahrt” (DLR) and was expanded to a stereoscopic system (SPIV). It consists of a double pulsed Nd:YAG-Laser (Quantel Twins,  $2 \times 150mJ$ ), two high resolution CCD-cameras (PCO Sencicam,  $1280px \times 1024px$ ) and an external sequencer (DLR). The good optical access to the test section from 3 sides allows PIV and SPIV measurements in all cartesian planes of the flow field. To minimize optical distortions (e.g. astigmatism) due to diffraction in water, the optical axis of the camera has to be aligned almost perpendicular to the border of the two optical media. Therefore, in case of SPIV measurements, water filled prisms (Ronneberger et al., 1998) or tanks with mirrors were mounted at the tunnel sidewalls to allow different viewing angles of up to  $\pm 45^\circ$  to the measurement volume.

### 3. DATA ACQUISITION AND ANALYSIS

LDA measurements were performed starting from the beginning of adverse pressure gradient until shortly beyond the onset of disturbance saturation. The resolution of the flow field in streamwise direction was  $Dx=10\text{ mm}$  in the transition region. In case of 3D disturbance input, the spanwise wave length was sampled with 16 boundary-layer profiles in spanwise direction. A wall normal step size of  $Dy=1\text{ mm}$  provided a resolution of boundary-layer profiles with about 25-30 points depending on the local boundary-layer thickness. The record length of all measured points was about 30 wire cycles. To evaluate the entire spectrum of the measured data time-signals were cut to multiples of the wire cycle. For an exact determination of amplitudes and phases of the fundamental frequency and its higher harmonics, a phase-averaging technique with respect to the TTL-signal of the disturbance source was used.

Due to long measurement times with LDA in water small structures cannot be sufficiently resolved. Here PIV (SPIV) with its high spatial resolution provides better results concerning the detection of structures in the transition region. Additionally, the third velocity component  $w$  can be measured, which is not accessible with the 2-component LDA. The recorded PIV data-sets have been dewarped (in case of SPIV) and evaluated with a FFT based cross-correlation method. A Levenberg-Marquardt peak-fitting algorithm provided sub-pixel accuracy and minimized peak-locking effects (Ronneberger et al, 1998). Unreasonable vectors (in general less than 2%-5%) were deleted and re-interpolated by a fit to their neighbours.

In case of amplitude measurements by PIV, the field of view was about  $58 \times 50\text{ mm}^2$ . With a sampling window size of  $32px \times 32px$  and  $16px$  step size, the resolution of wall normal boundary-layer profiles was up to 40-50 points and consequently higher than obtained by LDA measurements. To capture the fundamental frequency with its higher harmonics in case of 2-D disturbance input, phase-locked measurements in one  $xy$ -plane with respect to the disturbance source were carried out. The phase angle was shifted over 18 time-steps to sample one TS-period. For each phase angle 30 measurements were averaged. Due to the necessary spatial resolution in case of 3-D disturbance input, the flow field was scanned with the Laser light-sheet over one spacer wave-length  $\lambda_z$  for each phase angle. The light-sheet optics and the camera were mounted on two different traverses to move independently in spanwise  $z$ -direction. Due to this, the camera movement could be corrected because of diffraction in water. The traverses were coupled with the PIV system by a custom acquisition software (Labview). Therefore, data acquisition can be completely automated to record phase-locked data sets with spanwise resolution for one phase angle. According to LDA measurements, the step size in span was set to 16 positions over one spacer wave-length  $\lambda_z$ . For evaluation of mean boundary layer quantities, amplitude and phase distributions as well as amplification rates the same programs were used for the data-sets of both measurement techniques. In order to obtain temporal and spanwise wave numbers in case of 3-D disturbance input, a double Fourier transform in time and spanwise direction was applied. This yielded amplitudes  $a_{h,k}$  and phases  $F_{h,k}$  of the measured disturbance-wave combination. The indices  $h$  and  $k$  denote the wave-number coefficients in time and spanwise direction respectively. Below, the notation  $(h,k)$  will be used to specify the modes. This method can be used until small-scale and strong non-periodic 3D structures occur downstream disturbance saturation in the reattachment region of the laminar separation bubble.

### 4. RESULTS

In the present results the Reynolds number based on the displacement thickness at the separation line is  $Re_{\delta_1}=900$ . The extent of the laminar separation bubble of about  $270\text{ mm}$  is given by the mean dividing streamline (figure 3c) with the net mass flux set to zero (Fitzgerald and Müller, 1988).

$$\int_{y=0}^{\delta} \bar{u}(y) dy = 0$$

The first section of the LSB is dominated by a primary convective instability of the two-dimensional TS-wave (Maucher et al., 1999). Therefore, the development of the 2-D TS wave appears to be very important and is examined in detail. This shall be done in the following paragraphs for 2-D and 3-D disturbance input.

#### **4.1 2-D disturbance input, TS-wave**

A detailed comparison of boundary layer quantities from LDA measurements, LST and direct numerical simulations (DNS) under consideration of a 2-D disturbance input is given in Lang et al. (2000a) and Lang et al. (2000b). Very good agreement was obtained for base flow variables as well as for unsteady quantities. Now, PIV measurements were performed additionally in the region of linear amplification (according to LST) until beyond the onset of disturbance saturation. Obtained mean quantities and amplitude distributions will be compared to LST and LDA results in this section. To capture unsteady phenomena, phase-locked measurements were carried out (xy-plane). Averaging the whole data set over 18 measured time-steps yields base flow variables. Figure 3c shows very good agreement of the displacement thickness  $\delta_1$ , momentum loss thickness  $\delta_2$  and the dividing streamline in the saturation region, obtained from PIV data in comparison with LDA measurements.

It can be shown, that by phase-locked measurements the accuracy of PIV is sufficient not only to measure instantaneous data. It is also a suitable instrument to measure essentially small-amplitude ( $<5\%$  of the boundary layer edge-velocity  $u_d$ ) periodical phenomena. A Fourier analysis of 18 phase-averaged instantaneous boundary-layer profiles, shifted over one fundamental period as mentioned before, yields wall-normal amplitude distributions of the fundamental frequency (TS-wave) and its higher harmonics. For validation, a comparison with corresponding LDA-measurements of wall-normal amplitude distributions are given in figure 3a for three streamwise positions in the region of linear amplification (according to LST). Figure 3b shows the amplification of shear-layer maxima ( $u'_{max}$ ) obtained from PIV data with the amplification rate predicted by LST (normalized by  $u'_{max}(x=277\text{ mm})$ ). The amplification curve of this disturbance mode matches theory very well until the onset of saturation downstream  $x=310\text{ mm}$ . Here, a rapid 3D development starts, leading to 3-D breakdown of the separated shear layer, which cannot be described by LST.

The possibility of measuring unsteady phenomena by means of PIV has one important benefit. Measuring time of verification measurements for comparison with LST, to prove quality of the experimental set-up, could be decreased by more than a factor of 10 in comparison to adequate LDA measurements.

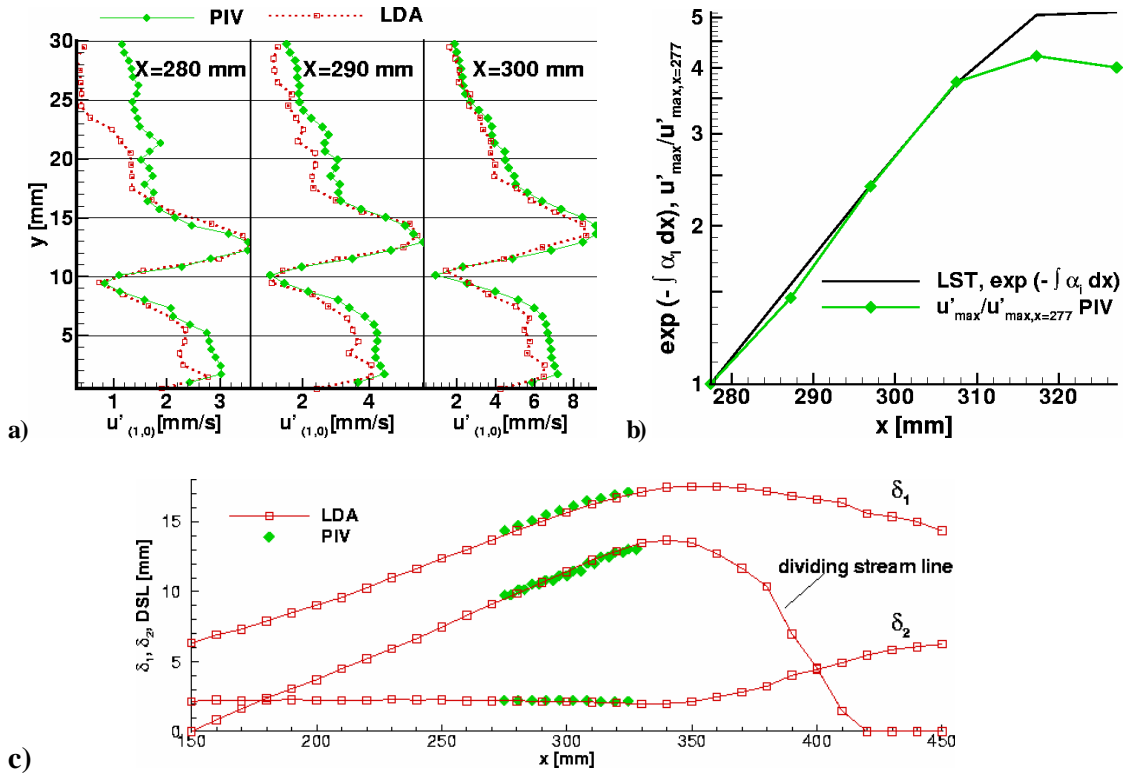


Fig. 3 Results from amplitude measurements by PIV with 2-D disturbance input (1,0-mode, TS-wave).  
a) Amplitude distributions  $u'(y)$  of the (1,0)-mode in comparison with corresponding LDA measurements in the region of linear (LST) disturbance amplification.  
b) Amplification of shear-layer maximum ( $u'_{\max}(x)/u'_{\max}(277\text{mm})$ , (1,0)-mode) in region of linear disturbance amplification (LST) until beyond disturbance saturation.  
c) Mean boundary-layer quantities measured by PIV in comparison with LDA data.

#### 4.2 3-D disturbance input

In case of 3-D disturbance input the oscillating wire is used in combination with spacers as described in section 2. This causes steady 3-D disturbances which, together with the TS-wave (2-D time harmonic), generate unsteady 3-D disturbance modes (oblique waves). Thus, the 2-D time harmonics are also included in case of 3-D disturbance input.

First, results from LDA measurements will be compared to LST and DNS (Marxen et al., 2002a). In the second part of this section PIV measured amplitude and phase distributions as well as disturbance amplification will be compared to LDA measurements and LST as described before for the 2-D case.

##### 4.2.1 Results from LDA measurements in comparison with LST and DNS

General properties of the LSB are first discussed using base-flow variables obtained from LDA-data in comparison with DNS. Here, base flow means averaged quantities in time and spanwise direction. Note that the LSB is a highly unsteady phenomenon as emphasised before, and the base flow can never be observed instantaneously at any time step. Due to this it appears inevitable to consider also time- and space-resolved disturbance quantities before claiming that the same physics are captured in the experimental and numerical investigations.

In figure 4a some boundary-layer quantities measured by LDA are shown for both cases of disturbance input (2-D and 3-D) in comparison with DNS. The boundary-layer displacement thickness  $\delta_1$  considerably

increases along the separation bubble, while the momentum-loss thickness  $\delta_2$  starts to grow not until the onset of transition. Good agreement between DNS results and measurements reveals that a separation bubble of approximately the same size is formed in both cases. As can be seen in figure 4a the boundary-layer parameters over the separated region are nearly the same for 2-D and 3-D disturbance input. The same holds for the size of the bubble, as can be also seen from investigations of Augustin et al. (2000). This confirms that the development of the 2-D TS wave is decisive for the transition process in the considered case and the disturbed steady 3-D mode (caused by spacers) does not play an important role. Therefore, in case of 3-D disturbance input the development of 2-D time harmonic quantities is examined in detail.

Figure 4b shows the amplification curve for amplitudes  $u'_{max}(x)$  normalized with the edge-velocity ( $u_{d,x=0mm}=174 \text{ mm/s}$ ) of the boundary-layer profile in the narrowest section. It can be seen that mode (1,0) (TS-wave) is strongly amplified in the region of the separated shear layer. Experimental and numerical results perfectly match from  $x=230 \text{ mm}$  onwards even shortly beyond saturation. Good agreement with linear stability theory (LST) confirms the primary convective nature of the disturbance (Maucher et al., 1999). Amplitude development predicted by LST is obtained by integrating amplification rates in streamwise direction. As can be seen from figure 4b, calculation and experiment also predict the same amplitude, growth rate and saturation level for the non-linearly generated higher harmonic disturbance (2,0). Both disturbances saturate at the position of shear-layer roll-up.

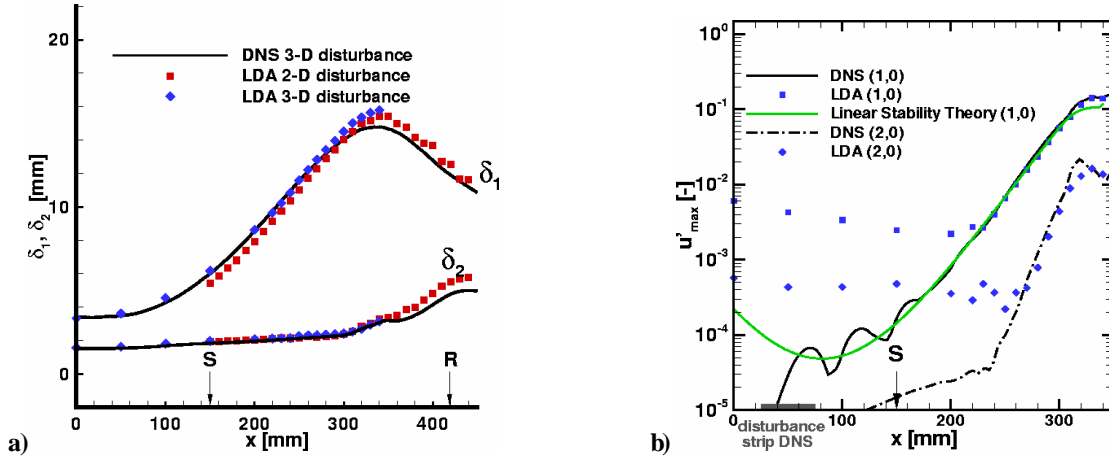


Fig. 4 Results from LDA measurements in comparison with DNS and LST (3-D disturbance input).

- a) Boundary-layer mean quantities over the whole separated region (S-R).
- b) Amplification of 2-D time harmonics ( $h,0$ -modes, TS-wave).

Wall-normal amplitude and phase distributions for both measured velocity components are compared to LST and DNS in figure 5 at a location around the middle of the region of linear amplification ( $x=290 \text{ mm}$ ). The detached shear-layer corresponds to the part of maximum gradient for the  $u$  velocity around  $y=13 \text{ mm}$ . It is at this distance from the wall where the disturbance amplitude  $u'(y)$  of the 2-D TS-wave (1,0-mode) reaches maximum values, as in the case of a Kelvin-Helmholtz instability. The measured amplitudes of these 2-D time harmonics perfectly match DNS results even for the first higher harmonic (2,0-mode). Shown amplitude distributions in figure 5 are normalized with the maximum amplitude  $u'_{max,(1,0)}$  of the TS-wave.

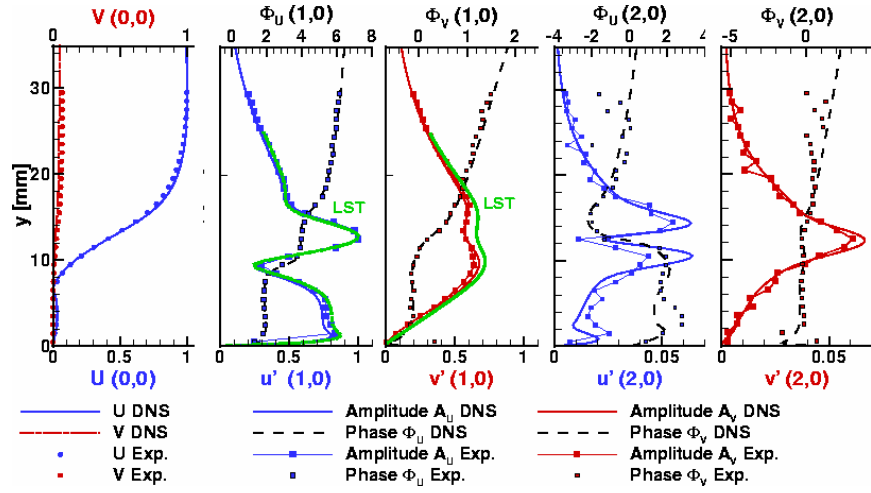


Fig. 5 Mean boundary-layer profiles (0,0) with wall normal amplitude and phase distributions of 2-D time harmonics ( $u$  and  $v$ ) by LDA in comparison with DNS and LST for streamwise position  $x=290$  mm.

In the experiment, a strong initial steady disturbance with half the spacer wavelength ( $0,2$ -mode) can be observed (figure 6a). From good agreement with LST for the development of the 2-D TS wave, as shown before, it can be concluded that the spanwise modulation of the base flow does not exert any influence on 2-D instability characteristics of the flow field. In contrast, the growth of spanwise modulated perturbations of fundamental frequency ( $1,\pm 2$ -modes) is decisively affected by the presence of this steady mode. The growth rate of these disturbances cannot be explained by linear theory, nor by a secondary (convective (Rist, 1998) or temporal (Maucher et al., 1999)) instability, since it already sets in well before the TS-wave has gained a sufficiently large amplitude. Instead, non-linear interaction between the TS-wave ( $1,0$ -mode) and the large steady disturbance ( $0,2$ ) with half the spacer wavelength, generates modes ( $1,\pm 2$ ) with approximately the same amplification rate as mode ( $1,0$ ). Results from a spanwise-symmetrical DNS confirm this fact by showing the same growth rate for mode ( $1,2$ ) only in the presence of a large steady disturbance. Agreement of amplitude and phase distributions between experiment and DNS is reasonable (figure 6b), albeit some deviations from symmetry can be seen in the measurements (figure 6a), which are not included in the DNS method.

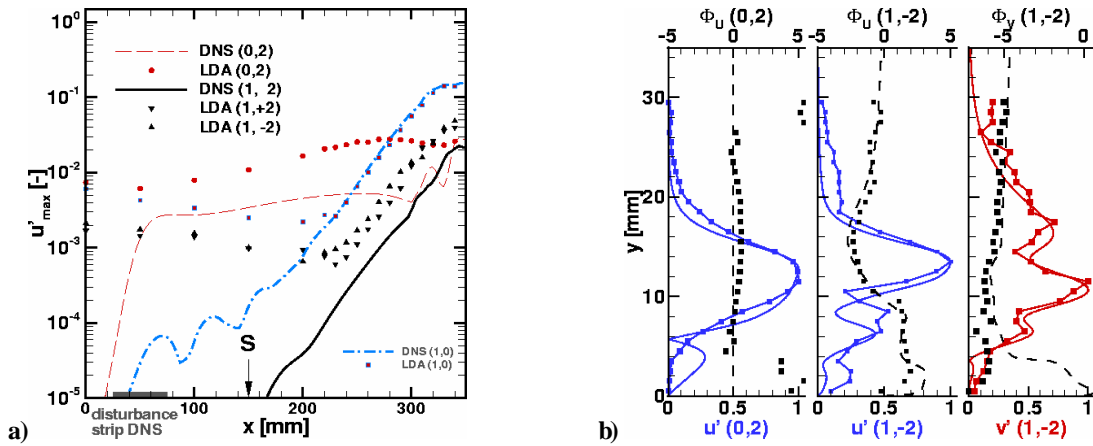


Fig. 6 Results from LDA measurements (symbols) in comparison with DNS (lines) under 3-D disturbance input.

a) Amplification of steady and unsteady 3-D disturbance modes in comparison with ( $1,0$ )-mode.

- b) Wall-normal amplitude and phase distributions of one steady  $(0,2)$  and unsteady  $((1,-2)$ , oblique wave) disturbance mode normalized with their maximum ( $x=290$  mm).

Despite the importance of three-dimensional disturbances for the breakdown to turbulence, the dominance of the two-dimensional fundamental perturbation even far downstream of reattachment is remarkable. Characteristics of the separation bubble have proven to be the same in a DNS with and without forced steady three-dimensional disturbances (Marxen et al., 2002a). The same holds for the experiment with and without spacers (see figure 4a), suggesting that the large initial disturbance level of three-dimensional disturbances plays only a minor role in the transition process. Instead, the dominating mechanism at work seems to be an absolute secondary instability of three-dimensional disturbances identified by Maucher et al. (1999) which is independent of the level of incoming 3-D disturbances (Marxen et al., 2002b). Hence, differences in amplitude and amplification of DNS and experiment for mode  $(0,2)$  are not critical.

#### 4.2.2 Results from PIV measurements in comparison with LDA and LST

In the region of linear disturbance amplification, mono-PIV measurements ( $xy$ -plane) were carried out to measure the development of the input 3-D wave combination. Phase-locked measurements shifted ( $\varphi=20^\circ$ ) over one period of the fundamental frequency (TS-wave) and in spanwise direction provide phase-averaged PIV data of instantaneous boundary-layer profiles as described in section 3. Results of the double Fourier transformed PIV data agree very well with corresponding LDA measurements.

Figure 7a shows mean boundary-layer quantities computed from LDA and PIV data. Therefore, the boundary-layer profiles were averaged in time and span ( $0,0$ -mode). An excellent agreement is achieved for mean quantities as well as for the amplification of velocity fluctuations ( $u'_{max}$ ) shown in figure 7b. The selected  $(h,k)$ -modes in figure 7b are dominant for the transition process in the considered case and have been already compared to DNS before. The very good agreement of unsteady disturbance development obtained from both measurement techniques applied, justifies the use of Mono-PIV for measurements of small-amplitude (periodic) phenomena. By applying the PIV technique instead of LDA, a significant decrease of measurement time can be achieved (by at least a factor of ten), although the measurement region is limited. With the application of a second camera, now available for stereoscopic measurements, the streamwise extend of the measurement region can be doubled.

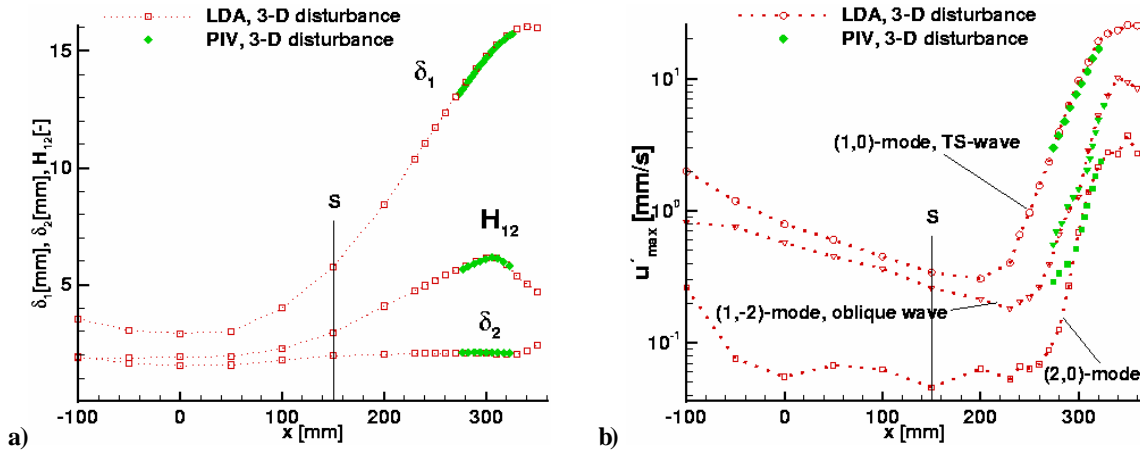


Fig. 7 Results of phase-locked mono-PIV measurements in comparison with LDA data (3-D disturbance input).

- a) Mean boundary-layer quantities.  
b) Amplification ( $u'_{max}$ ) of 2-D time harmonics and one 3-D disturbance mode (oblique wave) measured by mono-PIV in comparison with LDA data.

In figure 8a and 8b, a mean boundary-layer profile for the velocity component  $u$  together with wall-normal amplitude distributions ( $u$  and  $v$ ) for the TS-mode  $(1,0)$ -mode, obtained by the double Fourier transform, is

compared to LST at a single streamwise position ( $x=300$  mm) just before the onset of disturbance saturation. The results of LST are based on the measured mean velocity profile (averaged in time and span, figure 8a) which must be determined very accurately because its second derivative plays an important role according to the Orr-Sommerfeld equation. The very good agreement proves that the velocities and their fluctuations can be accurately determined from PIV data even in the region of strong velocity gradients within the shear layer.

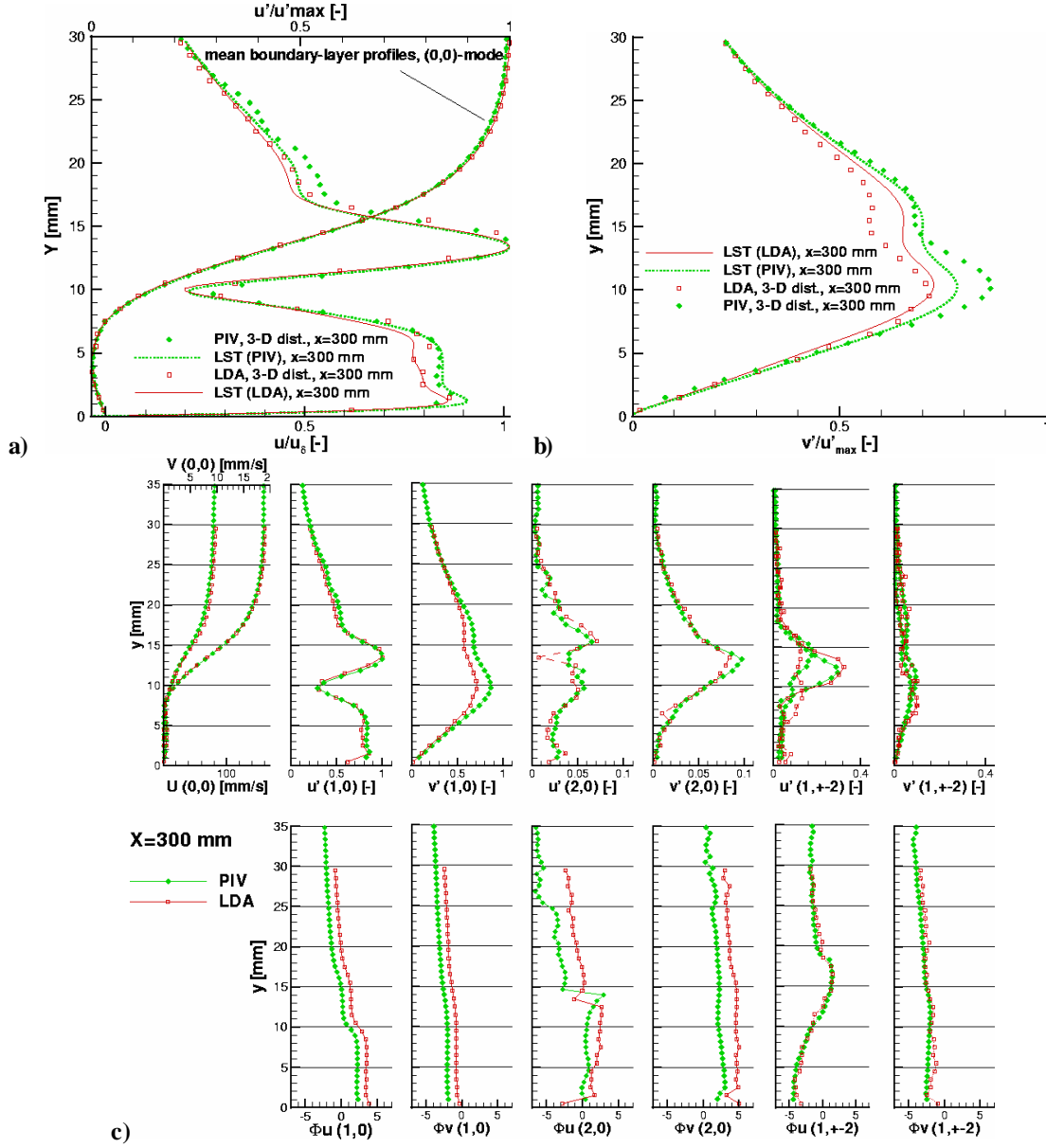


Fig. 8 Results from measurements of amplitude and phase distributions by mono-PIV (3-D disturbance input).

- Mean boundary-layer profile and wall-normal amplitude distribution (1,0-mode, TS-wave) from LDA and PIV measurements for velocity  $u$  in comparison with LST ( $x=300$  mm).
- Wall-normal amplitude distribution (1,0-mode, TS-wave) from LDA and PIV measurements for velocity  $v$  in comparison with LST ( $x=300$  mm).

- c) *Wall-normal amplitude and phase distributions (2-D time harmonics and oblique waves) from PIV measurements in comparison with LDA results for both measured velocity components ( $u$  and  $v$ ) at streamwise position  $x=300$  mm.*

Figure 8c shows a comparison of wall-normal amplitude ( $u'(y)$  and  $v'(y)$ ) and phase distributions ( $F_u(y)$  and  $F_v(y)$ ) for the disturbance modes illustrated in figure 7b. It is at the same streamwise position ( $x=300$  mm) as compared to LST in figure 8a and 8b. The amplitude distributions are normalized with the maximum amplitude  $u'_{max,(1,0)}$  of the TS-wave. It can be seen that even the higher harmonics ( $u'(2,0)$ ,  $v'(2,0)$ ) can be accurately measured by PIV, although their amplitude is less than 1% of the boundary layer's edge velocity  $u_d$  at this position.

#### 4.2.3 Results from stereoscopic PIV measurements

Despite a complicated set-up at a water-tunnel, because of diffraction effects between two optically different media, application of SPIV is superior to a mono-system concerning the detection of transitional structures, as can be seen in the following results. In the transition region with its strong 3-D development and bidirectional fluctuations, the possibility to capture all three velocity components simultaneously gives an additional insight into the 3-D breakdown of the separated shear layer. Figure 9a shows the average of 25 phase-locked SPIV measurements with the light sheet aligned parallel to the flat plate ( $y=16$  mm). Contour colours denote the out-of-plane component  $v$ . Rapid 3-D breakdown of the separated shear layer downstream the onset of saturation ( $x=310$  mm) under the occurrence of counter rotating vortex pairs is as clearly visible as the dominance of the TS wave, responsible for the strong vortex shedding in the transition region (figure 2b and 10b,  $xy$ -plane). In the vicinity of these counter rotating vortices, fluid is moved from inside the LSB up into the separated shear-layer (yellow and red contour colours, figure 9a) leading to 3-D breakdown. Due to strong velocity gradients in this region, first non-periodicities occur in the flow field, which means high *rms*-values when multiple measurements are averaged, as can be seen in figure 9b for the velocity component  $u$ .

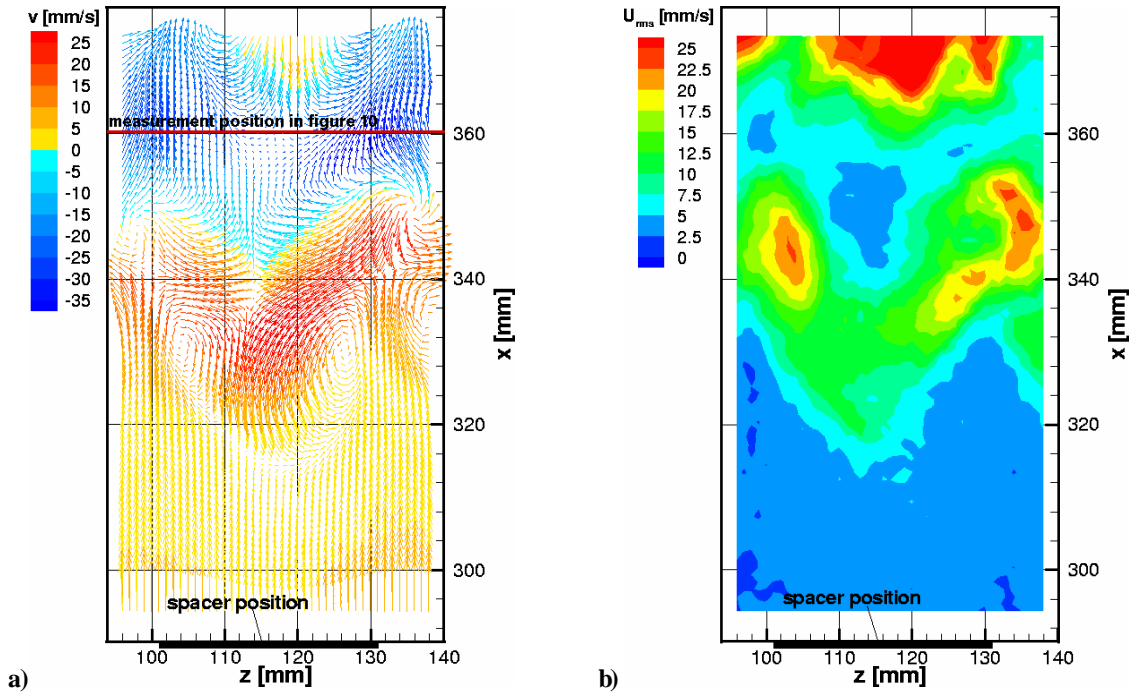


Fig. 9 Results from phase-locked stereoscopic PIV measurements in the  $xz$ -plane (light sheet aligned parallel to the flat plate,  $y=16$  mm).

- a) 3-D breakdown of the separated shear layer with counter-rotating vortex pairs. 25 measurements averaged. Red bar: measurement position of figure 10a.
- b) RMS results for velocity component  $u$  obtained by averaging 25 measurements (average shown in figure 9a). First non-periodicities in the regions of vortex pairs (high RMS values).

Figure 10a shows the average of 25 SPIV measurements in the  $yz$ -plane (perpendicular to the mean flow) at a streamwise position  $x=360$  (red bar in figure 9a). The measurements were taken phase-locked at equal phase angle as the measurement shown in figure 9. Again the out-of-plane component perpendicular to the light-sheet plane is denoted by colours (now velocity component  $u$ ). In the vicinity of counter-rotating vortex pairs a strong back flow can be detected (blue colours).

In figure 10b such a vortex pair can be seen from flow visualization (red ellipse). Here, fluid within the LSB (isolated by the dividing streamline) is orange coloured and one layer is additionally marked with a carpet of hydrogen bubbles (bright blue line). For this picture two laser light-sheets were aligned in streamwise direction ( $xy$ -plane) and perpendicular to the mean flow ( $yz$ -plane), respectively. In the  $xy$ -plane the roll-up of the separated shear layer can be seen, while the  $yz$ -plane shows the spanwise deformation with 3-D vortex structures in the transition region.

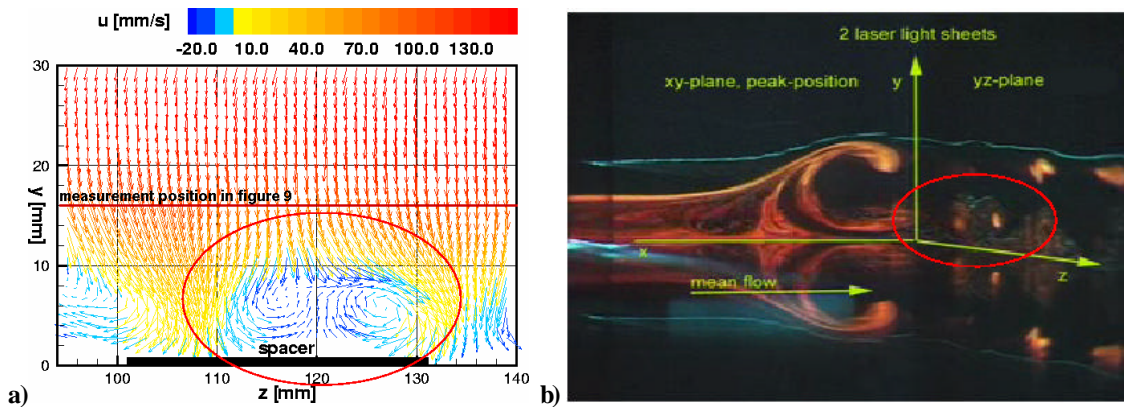


Fig. 10 Results from stereoscopic PIV measurements in the  $yz$ -plane (light sheet aligned perpendicular to the mean flow,  $x=360$  mm) and flow visualizations.

- a) Counter-rotating vortex pairs in the transition region of the LSB with strong back flow. Red bar: Measurement position in figure 9a.
- b) Vortex shedding in the transition region. Visualization with two perpendicular aligned Laser light-sheets ( $xy$ - and  $yz$ -plane). Fluid which is enclosed by the dividing streamline is orange coloured (instantaneous view). Bright line: hydrogen-bubble carpet as can be seen in figure 2.

## 5. CONCLUSIONS

A detailed investigation on transition in a laminar separation bubble is given. The onset of 3-D vortex structures causing the breakdown of a separated boundary layer was measured and visualized using phase-averaged LDA, phase-locked PIV and stereoscopic PIV. A method was shown to measure essentially small-amplitude phenomena and amplification of a 3-D disturbance wave. Comparisons with corresponding LDA measurements and linear stability theory agree very well. The possibility to measure unsteady phenomena using PIV lead to a significant decrease in measurement time compared to adequate LDA measurements.

LDA measurements could be compared also to direct numerical simulations. The velocity field of the transitional separation bubble shows very good agreement for time-averaged and 2-D Fourier-analyzed quantities. Transition in a separation bubble in the considered case is driven by convective primary amplification of 2-D TS waves, mainly determining the size and position of the bubble. The initial level of

steady 3-D disturbances in the inflow plays a minor role in the considered transition process. This could be clearly identified from the existing experimental and numerical data.

Stereoscopic PIV measurements gave new and closer insight into the 3-D development of the transitional shear layer. In the transition region with its strong bidirectional fluctuations vortex structures leading to 3-D breakdown could be measured which were up to now only accessible by qualitative flow visualizations or mono-PIV.

## REFERENCES

Augustin K., Rist U. and Wagner S., "Control of a Laminar Separation Bubble by Excitation of Boundary-Layer Disturbance Waves", In: Wagner, Rist, Heinemann and Hilbig (eds.), Notes on Numerical Fluid Mechanics, New Results in Numerical and Experimental Fluid Mechanics. 12<sup>th</sup> STAB Symposium 2000, Stuttgart, Springer Verlag, Heidelberg

Fitzgerald E.J. and Müller T.J. (1988), "Measurements in a Separation Bubble on an Airfoil Using Laser Velocimetry, AIAA Journal, 28(4)

Gaster M. (1966), "The Structure and Behaviour of Laminar Separation Bubbles, AGARD CP 4, pp. 813-854

Klebanoff P.S., Tidstrom K.D. and Sargent L.M. (1962), The Three-Dimensional Nature of Boundary Layer Instability, J. Fluid Mech. 12, pp.1-41

Kruse M. and Wagner S. (1996), "Measurements of Laminar-Turbulent Transition in a Flat-Plate Boundary Layer", Proc. 8<sup>th</sup> International Symposium of Laser Techniques to Fluid Mechanics, July, 8<sup>th</sup>-11<sup>th</sup>, Lisbon Portugal

Kruse M. (1997), "Einsatz der Laser-Doppler-Anemometrie zur Untersuchung des laminar-turbulenten Grenzschichtumschlags an der ebenen Platte", Dissertation, Universität Stuttgart

Lang M., Marxen O., Rist U. and Wagner S. (2000a), "Experimental and numerical Investigations on Transition in a Laminar Separation Bubble", In: Wagner, Rist, Heinemann and Hilbig (eds.), Notes on Numerical Fluid Mechanics, New Results in Numerical and Experimental Fluid Mechanics. 12<sup>th</sup> STAB Symposium 2000, Stuttgart, Springer Verlag, Heidelberg

Lang M., Marxen O., Rist U. and Wagner S. (2000b), "LDA-Messungen zur Transition in einer laminaren Ablöseblase", Proc. 8. Fachtagung der GALA, Lasermethoden in der Strömungsmesstechnik, Sept., 12<sup>th</sup>-14<sup>th</sup>, Freising-Weihenstephan Germany, Shaker Verlag, Aachen

Marxen O., Lang M., Rist U. and Wagner S. (2002a), "A Combined Experimental/Numerical Study of Unsteady Phenomena in a Laminar Separation Bubble", Proc. IUTAM Symposium "Unsteady Separated Flows" (CD-ROM), Toulouse

Marxen O., Rist U. and Wagner S. (2002b), "The Effect of Spanwise-Modulated Disturbances on Transition in a 2-D Separated Boundary Layer", Abstract submitted to the 41<sup>st</sup> AIAA Aerospace Sciences Meeting and Exhibit, January, 6<sup>th</sup>-9<sup>th</sup>, 2003, Reno, Nevada

Maucher U., Rist U. and Wagner S. (1999), "Transitional Structures in a Laminar Separation Bubble", In: W. Nitsche, H. Heinemann and R. Hilbig (eds.), Notes on Numerical Fluid Mechanics, vol. 72, pp. 307-314, Vieweg Verlag, Wiesbaden

Ronneberger O., Raffel M. and Kompenhans J. (1998), "Advanced Evaluation Algorithms for Standard and Dual Plane Particle Image Velocimetry", Proc. 9<sup>th</sup> International Symposium of Laser Techniques to Fluid Mechanics, July, 13<sup>th</sup>-16<sup>th</sup>, Lisbon Portugal

Spalart P.R. and Strelets M.Kh. (2000), "Mechanisms of Transition and Heat Transfer in a Separation Bubble", *J. Fluid Mech.*, 403, pp. 329-349

Strunz, M. and Speth J.F. (1987), "A New laminar Water-Tunnel to Study the Transition Process in a Blasius Boundary Layer and in a Separation Bubble and a New Tool for Industrial Aerodynamics and Hydrodynamic Research", AGARD CP-413, pp. 25-1 – 25-5

Watmuff J. (1999), "Evolution of a Wave Packet into vortex Loops in a Laminar separation Bubble", *J. Fluid Mech.*, 397, 119-169

Westerweel J. and van Oord, J. (2000), "Stereoscopic PIV measurements in a Turbulent Boundary Layer", In: Stanislas M.; Kompenhans J.; Westerweel J. (eds.), *Particle Image velocimetry; Progress toward Industrial Application*

Wiegand Th. (1997), "Experimentelle Untersuchungen zum laminar-turbulenten Transitionsprozess eines Wellenzuges in einer Plattengrenzschicht, Dissertation, Universität Stuttgart